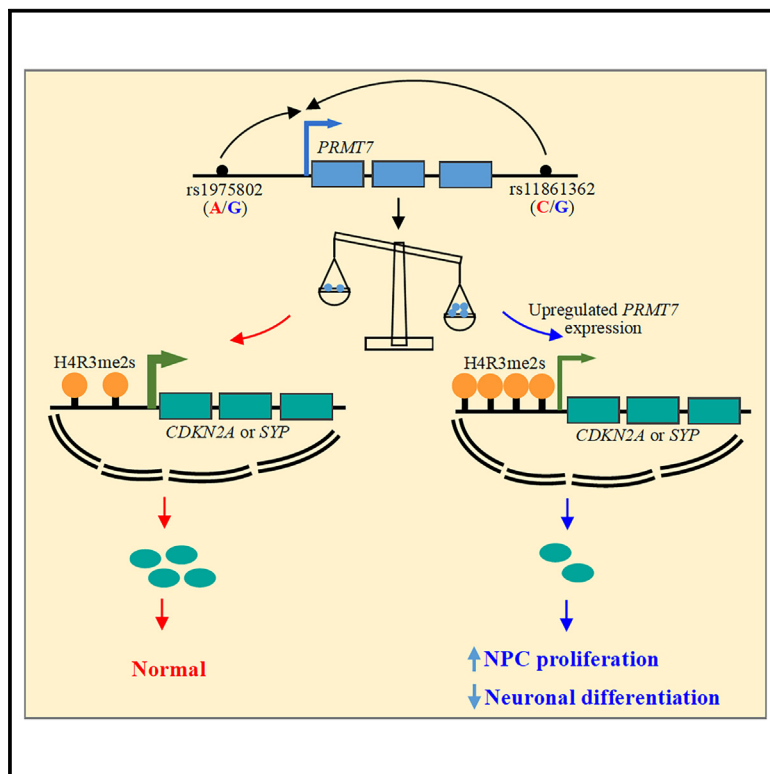


Protein arginine methyltransferase 7 linked to schizophrenia through regulation of neural progenitor cell proliferation and differentiation

Graphical abstract



Authors

Ting Shen, Jing Yu, Bin Xie, ..., Kefu Liu, Chunyu Liu, Chao Chen

Correspondence

shenting200849@126.com (T.S.), chenchao@sklimg.edu.cn (C.C.)

In brief

Shen et al. documented that *PRMT7* is a functional target of SCZ risk SNPs at 16q22.1. They further uncovered that *PRMT7* dysregulation resulted in NPC function defects by impacting the expression of genes related to the cell cycle and neuronal function, potentially contributing to the risk of SCZ.

Highlights

- *PRMT7* acts as a downstream target of the SCZ risk SNPs rs1975802 and rs11861362 at 16q22.1
- *PRMT7* depletion reduced NPC growth and boosted neuronal differentiation in 2D and 3D models
- *PRMT7* regulates the expression of *CDKN2A* and *SYP* via H4R3me2s modification of their promoters



Article

Protein arginine methyltransferase 7 linked to schizophrenia through regulation of neural progenitor cell proliferation and differentiation

Ting Shen,^{1,6,*} Jing Yu,^{1,6} Bin Xie,^{1,6} Cuiping Huang,¹ Jingjie Cui,¹ Kefu Liu,¹ Chunyu Liu,^{1,2} and Chao Chen^{1,3,4,5,7,*}

¹MOE Key Laboratory of Rare Pediatric Diseases & Hunan Key Laboratory of Medical Genetics, School of Life Sciences, and Department of Psychiatry, The Second Xiangya Hospital, Central South University, Changsha 410000, Hunan, China

²Department of Psychiatry, SUNY Upstate Medical University, Syracuse, NY, USA

³National Clinical Research Center for Mental Disorders, The Second Xiangya Hospital, Central South University, Changsha 410000, Hunan, China

⁴Furong Laboratory, Changsha 410000, Hunan, China

⁵Hunan Key Laboratory of Animal Models for Human Diseases, Central South University, Changsha 410000, China

⁶These authors contributed equally

⁷Lead contact

*Correspondence: shenting200849@126.com (T.S.), chenchao@sklmg.edu.cn (C.C.)

<https://doi.org/10.1016/j.celrep.2025.115279>

SUMMARY

Genome-wide association studies (GWASs) have identified numerous genomic loci linked to schizophrenia (SCZ), while their pathogenic mechanisms largely remain unclear. This study demonstrated protein arginine methyltransferase 7 (PRMT7) as a key target of SCZ risk SNPs with allele-specific enhancer activity at 16q22.1. Downregulating PRMT7 in neural progenitor cells (NPCs) decreased proliferation, increased neuronal differentiation, and also led to longer neurites in these neurons. Conversely, overexpressing PRMT7 enhanced NPC proliferation and reduced neuronal differentiation. In three-dimensional (3D) cerebral organoids, similar NPC phenotypic changes were noted following PRMT7 depletion. Mechanistically, PRMT7 regulates the expression of genes related to the cell cycle and neuronal functions, such as CDKN2A and SYP, via symmetrical di-methylation at arginine 3 of histone 4 (H4R3me2s) modification in their promoters. Notably, these genes have a stronger association with SCZ compared to other mental disorders. Together, the results of this study reveal that PRMT7 is a functional gene at 16q22.1, contributing to the etiology of SCZ by modulating NPC proliferation and differentiation as an epigenetic regulator.

INTRODUCTION

Schizophrenia (SCZ) is accepted as a neurodevelopment disorder with strong heritability and complex inheritance, which affects about 1% of the population worldwide.¹ Based on genome-wide association studies (GWASs), many genomic loci associated with SCZ have been successfully identified.² Remarkably, most of the risk SNPs within these loci reside in the non-coding regions usually harboring regulatory functions, implying that these loci may be involved in SCZ pathogenesis by modulating the transcription of downstream genes via regulators, such as enhancer and promoter contacts.^{3–5}

To uncover loci contributing to illness through genetically regulated expression, gene-based strategies integrating GWAS summary statistics and expression quantitative trait loci (eQTLs), such as transcriptome-wide association studies (TWASs), have been applied to SCZ.^{6–11} These TWAS-identified SCZ-associated genes are significantly enriched in neurodevelopment-related pathways, favoring the neurodevelopmental pathophysiology of SCZ.^{8,9}

In this study, we prioritized one member of protein arginine methyltransferases (PRMTs), PRMT7, at the chromosomal region 16q22.1 for SCZ susceptibility by integrating the published TWAS results.^{7–9,12} Moreover, the SCZ risk SNPs in this locus were identified to have enhancer activity and regulate PRMT7 expression. Further investigation showed that PRMT7 played a critical role in neural progenitor cell (NPC) proliferation and neuronal differentiation during the development of cerebral organoids, possibly via regulating the expression of genes involved in the cell cycle and neuronal function. These results support the contribution of PRMT7 to SCZ risk.

RESULTS

PRMT7 is identified as one of the SCZ risk genes

Several SCZ-associated susceptibility SNPs are located at 16q22.1 with high significance, including rs8044995,¹³ rs1975802,¹⁴ rs3743739,^{15,16} rs11861362,¹⁶ and rs11862968.¹⁷ All of these SNPs are supported by GWASs or meta-analyses of GWASs (details in Table S1). *Cis*-eQTL analysis showed that



these SNPs were significantly associated with the expression of *PRMT7* in various GTEx brain tissues, including frontal cortex (Figures 1A, 1B, and S1A–S1C). Another dataset, from the Lieber Institute for Brain Development (LIBD), also supported these associations in dorsolateral prefrontal cortex (DLPFC) (Figures S1D–S1H; Table S2). The results imply that *PRMT7* may be the target gene of these SCZ-associated SNPs.

To confirm the relationship between *PRMT7* and SCZ, we further analyzed the published TWAS datasets.^{7,8,10,12} These data also consistently supported *PRMT7* as the candidate risk gene of SCZ (Table S3). Moreover, data in the BrainEXP-NPD, including gene expression profiles in the brains of six kinds of neuropsychiatric disorders, show that *PRMT7* is significantly differentially expressed in patients with SCZ compared to controls (nominal $p = 1.0 \times 10^{-3}$, false discovery rate [FDR] $q = 1.1 \times 10^{-2}$).¹⁸

Among all the GWAS- and TWAS-involved SNPs, rs3785113 and rs79543001 show the strongest associations with *PRMT7* expression. Therefore, we planned to investigate how they regulated *PRMT7* expression. These two SNPs are in strong linkage disequilibrium (LD) with the risk SNPs rs11861362 and rs11862968 ($r^2 > 0.6$). Additionally, the other three SCZ risk SNPs, rs8044995, rs1975802, and rs3743739, were in the same LD block ($r^2 > 0.6$). Further analysis indicated that the rs11861362- and rs1975802-residing region contains signals of enhancer-specific histone modification mono-methylation at lysine 4 of histone 3 (H3K4me1) and acetylation at lysine 27 of histone 3 (H3K27ac), DNase I hypersensitive sites, and transcription factor (TF) binding sites (Figures S2A and S2B). In addition, the chromosomal conformation capture experiment in the brain region from the public dataset showed that there is an interaction between the two SNP-residing regions and the *PRMT7* promoter (Figures S2C and S2D). Hence, we next focused on investigating the effects of rs11861362 and rs1975802 on regulating *PRMT7* expression.

We first performed dual-luciferase assays in SH-SY5Y and NPCs to verify the regulatory function of the two SNP-located regions. The results showed that the sequence containing rs1975802 or rs11861362 did have enhancer activity with allelic specificity, consistent with the *cis*-eQTL (Figures 1C–1E and S2E–S2H). To confirm that *PRMT7* is the target of rs1975802 and rs11861362, we first inserted the SNP-residing region upstream of the *PRMT7* promoter in the pGL3-basic luciferase vector (Figure 1F). Dramatically increased luciferase activity was observed in the constructs with the SNP-residing region compared to the control, and this activity was also allele specific (Figures 1G and 1H). We further utilized the CRISPR-dCas9 strategy to examine their relationship. The dCas9 can suppress or promote the regulatory activity of its targeting region through the KRAB inhibitory domain (CRISPRi) or VP48 active domain (CRISPRa). *PRMT7* expression was significantly reduced in CRISPRi when the dCas9 was guided by small guide RNA (sgRNA) to bind the region, rs1975802 or rs11861362, it resided in (Figures 1I and 1J). In contrast, the higher expression of *PRMT7* was observed in CRISPRa for both rs1975802 and rs11861362 (Figures 1K and 1L).

Collectively, these results genetically indicated that *PRMT7* was associated with SCZ susceptibility by serving as the target of the SCZ risk SNPs at 16q22.1.

PRMT7 modulates the function of NPCs in 2D cultures

The mutation occurrence to *PRMT7* causes individuals to undergo abnormal developmental phenotypes, including intellectual disability, suggesting that *PRMT7* may play a significant role in brain development.^{19–21} Therefore, we speculated that *PRMT7* may lead to SCZ risk by modulating neural development. In this study, we first explored the effects of *PRMT7* on the proliferative and differential ability of NPCs in two-dimensional (2D) cultures.

The NPCs used in this study were derived from the induction of human embryonic stem cell line H9, both of which have been characterized by specific expression markers, such as TRA-1-60 and optimal cutting temperature (OCT) immunostaining for H9 and NESTIN and PAX6 for NPCs (Figures S3A–S3D). At first, we downregulated *PRMT7* expression in NPCs via short hairpin RNA (shRNA), which is transduced into cells by lentivirus (Figures 2A and 2B). These cells with *PRMT7* depletion displayed decreased proliferation ability compared to the control (Figures 2C–2E). Next, the NPCs with or without *PRMT7* knockdown were induced into neurons and astrocytes. The number of differentiated neurons from NPCs was significantly increased upon *PRMT7* downregulation detected at day 15 (Figures 2F and 2G), while astrocyte differentiation was not affected when *PRMT7* was knocked down (Figures S3E and S3F). Additionally, the neurons with the reduction of *PRMT7* expression exhibited elongated neurites relative to the control (Figure 2H). Then, we pharmaceutically suppressed the enzymatic activity of *PRMT7* in NPCs by using its specific inhibitor SGC3027 (Figures S3G and S3H). We observed that these cells also showed reduced proliferation rates compared to the control (Figure 2I). Additionally, the higher concentration level of SGC3027 caused a more severely decreased cell growth ability (Figure 2I). Moreover, the EdU experiment provided additional support that *PRMT7* inhibition suppressed cell proliferation (Figures 2J and 2K).

Next, we replicated the above functional experiments in another NPC, which is derived from the differentiation of U1M, an induced pluripotent stem cell (iPSC) line. Consistently, these NPCs had decreased proliferation and increased neuronal differentiation when *PRMT7* was downregulated (Figures S4A–S4G). Additionally, the neurite exhibited longer length when comparing *PRMT7*-depleted cells to the control (Figures S4F and S4H). Besides, when *PRMT7* enzyme activity was suppressed by its specific inhibitor SGC3027, CCK-8 and EdU assays showed that the NPCs underwent reduced proliferation (Figures S4I–S4L).

To further explore *PRMT7*'s function in NPCs, we performed *PRMT7* overexpression in both H9- and U1M-induced NPCs and then examined their proliferation and neuronal differentiation. On the contrary, these cells with *PRMT7* upregulation showed increased proliferation and decreased neuronal differentiation compared to the control (Figures S5A–S5G and S5L–S5R). Additionally, when we used SGC3027 to treat the cells with *PRMT7* upregulation, the proliferation of these cells remarkably decreased compared to that of *PRMT7*-overexpressed cells without treatment (Figures S5H–S5K and S5S–S5V).

The above results indicated that *PRMT7* plays a critical role in NPCs' proliferation and differentiation into neurons.

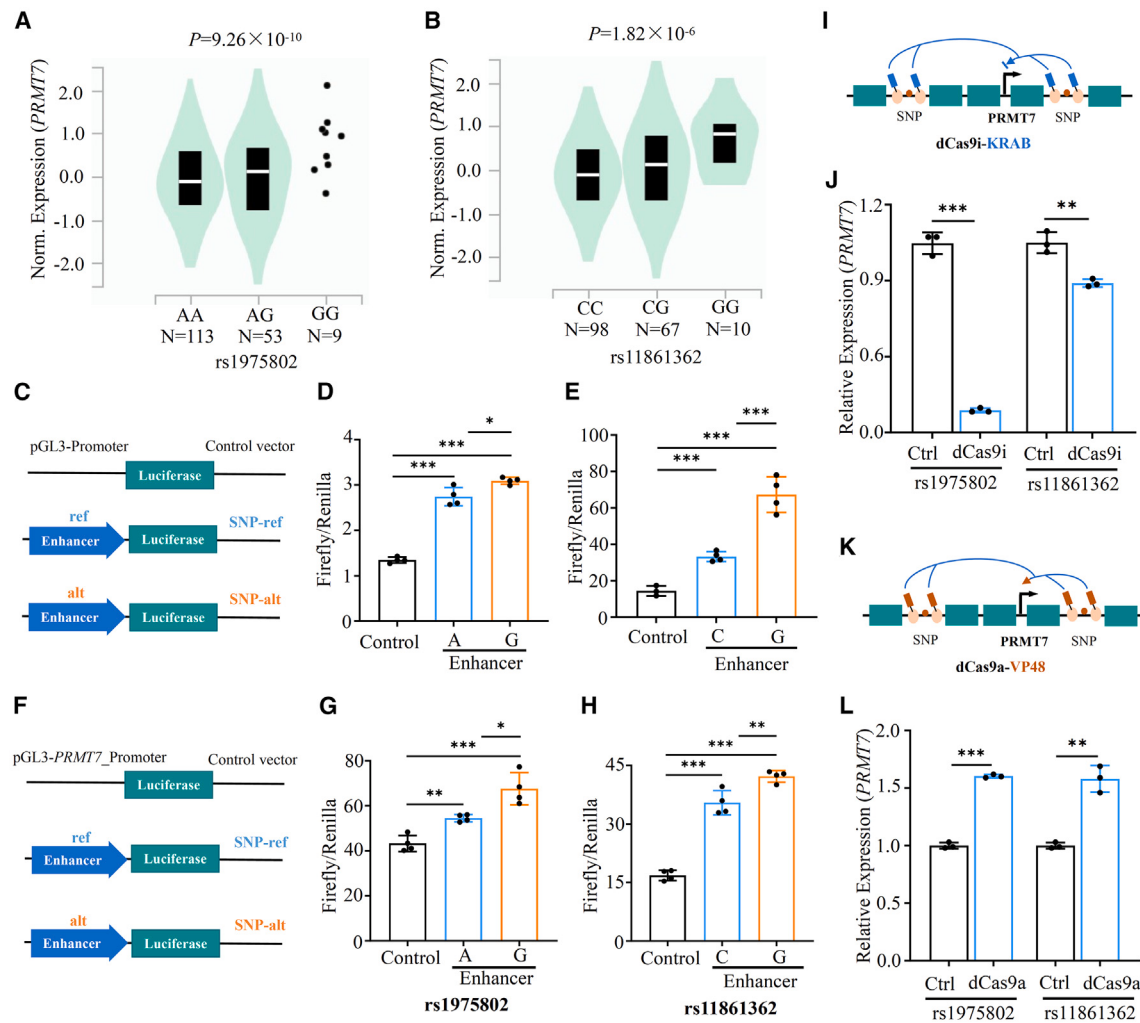


Figure 1. SCZ risk SNPs regulate *PRMT7* expression via enhancer activity

(A and B) *Cis*-eQTL analysis for the association of rs1975802 (A) or rs11861362 (B) with *PRMT7* expression in GTEx frontal cortex tissues, respectively. The genotype of rs1975802 in individuals corresponds to AA, AG, and GG, respectively. GG, CG, and CG correspond to the genotype of rs11861362 in individuals. N means the number of samples harboring this genotype. The eQTL plots were downloaded from the GTEx portal (<https://www.gtexportal.org/home/>).

(C–E) Dual-luciferase assays for the enhancer activity of rs1975802- or rs11861362-residing region. The sequence containing each allele of rs1975802, A or G, and rs11861362, C or G, is individually cloned into a pGL3-promoter vector (C). Their enhancer activity is quantified by normalizing the Firefly luciferase value to the Renilla (D and E). For rs1975802, $p < 0.0001$ in enhancer-A or enhancer-G compared to control (Ctrl) and $p = 0.0180$ in enhancer-G compared to enhancer-A. For rs11861362, $p = 0.0003$ in enhancer-C or enhancer-G compared to Ctrl and $p = 0.0005$ in enhancer-G compared to enhancer-C. Values are expressed by the mean \pm SD; $n = 4$ in (D) and (E).

(F–H) Dual-luciferase assays for the potential interaction of rs1975802- or rs11861362-residing enhancer with *PRMT7* promoter. The sequence with each allele of rs1975802, A or G, and rs11861362, C or G, is separately cloned upstream of the *PRMT7* promoter (F), and then Firefly and Renilla luciferase activities are successively detected (G and H). The Renilla luciferase value acts as the internal Ctrl. For rs1975802, $p = 0.0013$ and 0.0009 in enhancer-A and enhancer-G compared to Ctrl, respectively, and $p = 0.0117$ in enhancer-G compared to enhancer-A. For rs11861362, $p < 0.0001$ in enhancer-C or enhancer-G compared to Ctrl and $p = 0.0077$ in enhancer-G compared to enhancer-C. Values are expressed by the mean \pm SD; $n = 4$ in (G) and (H).

(I–L) CRISPR-dCas9 for the confirmation of the regulation of rs1975802- or rs11861362-residing enhancer on the expression of *PRMT7*. The dCas9 with repressive domain KRAB (dCas9i) (I) or active domain VP48 (dCas9a) (K) binds to the nearby regions of rs1975802 or rs11861362, and then the relative expression of *PRMT7* is quantified by RT-qPCR (J and L). For dCas9i, $p < 0.0001$ and $p = 0.0034$ in dCas9i-rs1975802 and dCas9i-rs11861362 compared to Ctrl, respectively. For dCas9a, $p < 0.0001$ and $p = 0.0011$ in dCas9a-rs1975802 and dCas9a-rs11861362 compared to Ctrl, respectively. Values are expressed by the mean \pm SD; $n = 3$ in (J) and (L).

* $p < 0.05$, ** $p < 0.01$, and *** $p < 0.001$ (two-sided Student's t test).

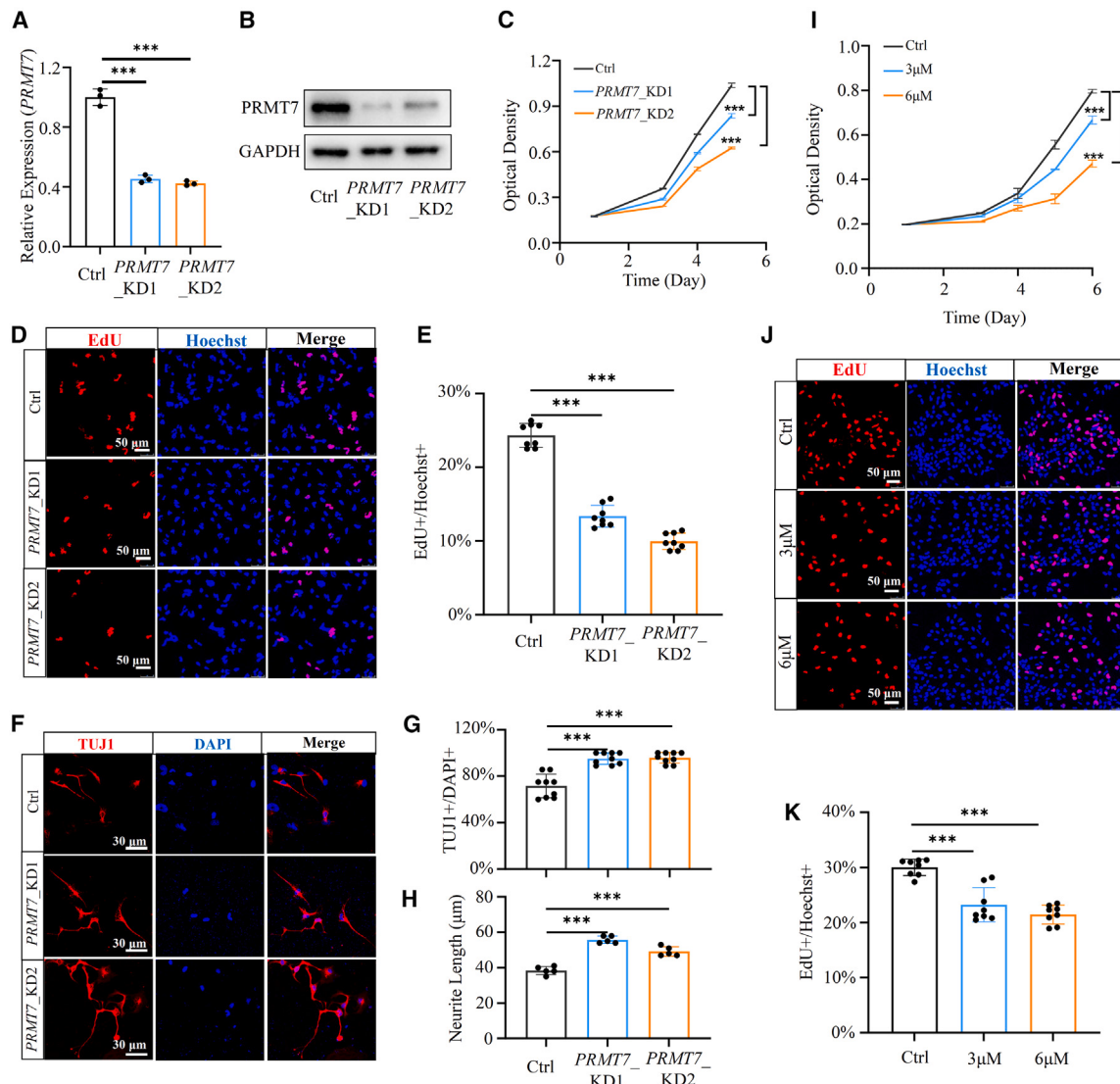


Figure 2. PRMT7 regulates the proliferation and differentiation of NPCs in 2D cultures

(A and B) RT-qPCR (A) and western blot (B) for the detection of PRMT7 expression level in NPCs with *PRMT7* knockdown and the control cells. GAPDH acts as the internal control. $p = 0.0001$ and $p < 0.0001$ in *PRMT7*_KD1 and *PRMT7*_KD2 compared to Ctrl, respectively. Values are expressed as mean \pm SD; $n = 3$ in (A). (C) The growth curve of *PRMT7*-depleted cells and the control assayed via CCK-8 kit. $p < 0.0001$ in *PRMT7*_KD1 or *PRMT7*_KD2 compared to Ctrl at day 5. Values are expressed as mean \pm SD; $n = 3$.

(D) EdU immunostaining for the detection of proliferative cells in *PRMT7*-downregulated cells and the control.

(E) The cells with EdU staining are counted and normalized to the total cells marked by Hoechst. Eight pictures for each group are included to be calculated. $p < 0.0001$ in *PRMT7*_KD1 or *PRMT7*_KD2 compared to Ctrl. Values are expressed as mean \pm SD; $n = 8$.

(F–H) Immunostaining of TUJ1. The differentiated neurons at day 15 of NPC induction are stained by the marker TUJ1 (F), and their occupancy is quantified by the number of neurons marked by TUJ1 compared to that of the total cells marked by DAPI (G). Nine pictures for each group are included to be calculated. $p < 0.0001$ in *PRMT7*_KD1 or *PRMT7*_KD2 compared to Ctrl. Values are expressed as mean \pm SD; $n = 9$. Additionally, the length of the neurite is measured in *PRMT7*-knockdown cells and the control via ImageJ software (H). Five pictures for each group are included to be calculated. $p < 0.0001$ and $p = 0.0001$ in *PRMT7*_KD1 and *PRMT7*_KD2 compared to Ctrl, respectively. Values are expressed as mean \pm SD; $n = 5$.

(I) CCK-8 assay for cell growth before and after the inhibition of PRMT7 enzymatic activity by the specific antagonist SGC3027. The control cells are treated by DMSO. $p < 0.0001$ in 3 or 6 μ M compared to Ctrl at day 6. Values are expressed as mean \pm SD; $n = 3$.

(J and K) EdU immunostaining in cells treated by SGC3027 or not. The proliferative cells are marked by EdU (J), and the quantification is performed by comparing the number of EdU-positive cells to that of Hoechst-positive cells (K). Eight pictures for each group are included to be calculated. $p < 0.0001$ in 3 or 6 μ M compared to Ctrl. Values are expressed as mean \pm SD; $n = 8$.

*** $p < 0.001$ (two-sided Student's t test).

PRMT7 regulates neural development in 3D cerebral organoids

To deeply explore the regulatory effects of PRMT7 on the neurodevelopmental processes, we planned to use the 3D cerebral organoids, which mimic early embryonic brain development with a high degree of accuracy, for further investigation. The H9 cells with *PRMT7* downregulation and the control cells were individually induced into the cerebral organoids. These cells successfully developed into the cerebral organoids (Figures 3A, 3B, and S6A), while the organoids with downregulated *PRMT7* showed a relatively slow growth rate and a small size following the increasing culture time compared to the control (Figures S6B–S6D).

Firstly, we examined the proliferation ability of NPCs with or without *PRMT7* knockdown through immunostaining with the proliferation marker Ki67 and EdU assay at day 20. The NPCs in these organoids had a decreased proliferation when *PRMT7* was downregulated (Figures 3C–3F). Next, we also examined the neuronal differentiation in this model. The number of neurons indicated by TUJ1 and TBR1 significantly increased in cerebral organoids with *PRMT7* knockdown at day 30, consistent with the observation at the 2D level (Figures 3G and 3H).

We also induced U1M with *PRMT7* downregulation or not to form cerebral organoids. At day 20, we found that the cerebral organoids with *PRMT7* downregulation also showed reduced proliferation (Figures S7A–S7F). Additionally, the increased number of neurons was observed when we performed immunostaining of TUJ1 and TBR1 at day 30 (Figures S7G–S7J).

These results suggested that *PRMT7* dysregulation may disturb the NPC proliferation and neuron differentiation during brain development.

PRMT7 is involved in SCZ by regulating the expression of cell cycle- and neuronal-function-related genes

Next, we aimed to unveil the molecular infrastructures of how *PRMT7* is linked to SCZ risk by performing RNA sequencing (RNA-seq) in NPCs with and without *PRMT7* knockdown. 345 shared differentially expressed genes (DEGs) were identified by comparing *PRMT7*-downregulated groups to the controls according to the following criteria: $p < 0.05$ and $|log_2 \text{ fold change (FC)}| \geq 0.6$ (Figure 4A). Then, we randomly selected 20 genes from these DEGs and validated their expression change by RT-qPCR in *PRMT7*-depleted NPCs and the control (Figures 4B and 4C). Additionally, most of these genes (17/20) also underwent similar expression changes when *PRMT7* activity was inhibited by SGC3027 in NPCs (Figures S8A and S8B).

Next, the functional enrichment analysis showed that the DEGs were mainly associated with the cell cycle (Figure 4D), with significant enrichment in DNA-replication-related pathways, as well as cell-division-related signatures, like the Wnt signaling pathway, recognized as a critical player in controlling G1/S progression of cell division. Additionally, there was a significant enrichment of the neuronal-function-associated signatures, including sensory perception of pain, negative regulation of action potential, cell adhesion molecules, and neuroactive ligand-receptor interaction (Figure 4D). Moreover, of the DEGs, the downregulated genes were primarily enriched in the cell cycle, while the upregulated genes are mainly related to the neuronal function (Figures S8C and S8D). These results indicated that

the genes related to the cell cycle and neuronal function are more possibly under-regulated by *PRMT7* during neural development.

Then, we explored which genes may be the direct downstream effectors of *PRMT7* and how *PRMT7* modulated their expression. Through the construction of the protein-protein interaction (PPI) network of these DEGs, we found that *CDKN2A*, as a critical suppressive regulator of cell cycle progression, and *SYP*, an integral membrane protein of small synaptic vesicles, were located at the center of this network (Figure 4E), providing additional support for the above results and implying they might be the key targets of *PRMT7*. As an arginine methyltransferase, *PRMT7* has been well studied and is known to be involved in the regulation of gene expression by depositing symmetrical di-methylation at arginine 3 of histone 4 (H4R3me2s), a repressive chromatin modification, on genes' promoter regions via co-operating with *PRMT5*.²² Notably, we found that the abundance of H4R3me2s was significantly decreased in *PRMT7*-downregulated NPCs and H9 compared to the control (Figures 4F, S8E, and S8F). Additionally, we found that the promoter regions of *CDKN2A* and *SYP* harbor the motifs "CAGCTG" and "CACGTG," which are core sequences for H4R3me2s modification. For *CDKN2A*, there are three H4R3me2s motifs individually distributed on the promoter of its two transcript isoforms, *INK4A* and *ARF*, both of which have a common function in cell cycle control (Figure 4G). For *SYP*, one H4R3me2s motif resides on the promoter region (Figure 4H). Next, chromatin immunoprecipitation of H4R3me2s coupled with qPCR (ChIP-qPCR) confirmed that there was indeed an H4R3me2s modification on these two genes' promoter regions (Figures 4G and 4H). Consistently, as shown in RNA-seq analysis and RT-qPCR assay, the expression of *CDKN2A*, including its two isoforms, and *SYP* were upregulated when *PRMT7* expression was downregulated or its function was inhibited (Figures 4A, 4C, S8B, S8G, and S8H). Therefore, these combined results indicated that *PRMT7* may directly regulate the expression of *CDKN2A* and *SYP* via H4R3me2s.

We further examined that there was a close relationship of *PRMT7*-regulated DEGs with mental disorders (Figure S8). Hence, we then introduced datasets of four mental-disorder-associated genes from the PsychENCODE consortium. PsychENCODE data include DEGs from postmortem brain samples of patients with autism spectrum disorder (ASD), bipolar disorder (BD), major depressive disorder (MDD), and SCZ⁷ (Table S4). With enrichment analysis, we found that *PRMT7*-regulated DEGs showed a significant enrichment in SCZ (Figure 4I). Then, we specifically downloaded other data of SCZ-associated genes also derived from an *in vitro* culture model by comparing genes' expressions in iPSC-derived 3D cerebral organoids from patients with SCZ to those in the control, called SCZ organoid DEGs (Table S5).⁴ Also, a significant enrichment of our DEGs in this dataset was observed (Figure 4J). Additionally, these shared genes were also prominently enriched in signatures of cell proliferation and the Wnt signaling pathway (Figure 4K).

Together, these results indicated that *PRMT7* may be involved in SCZ pathogenesis by regulating the expression of cell cycle- and neuronal-function-related genes via H4R3me2s modification.

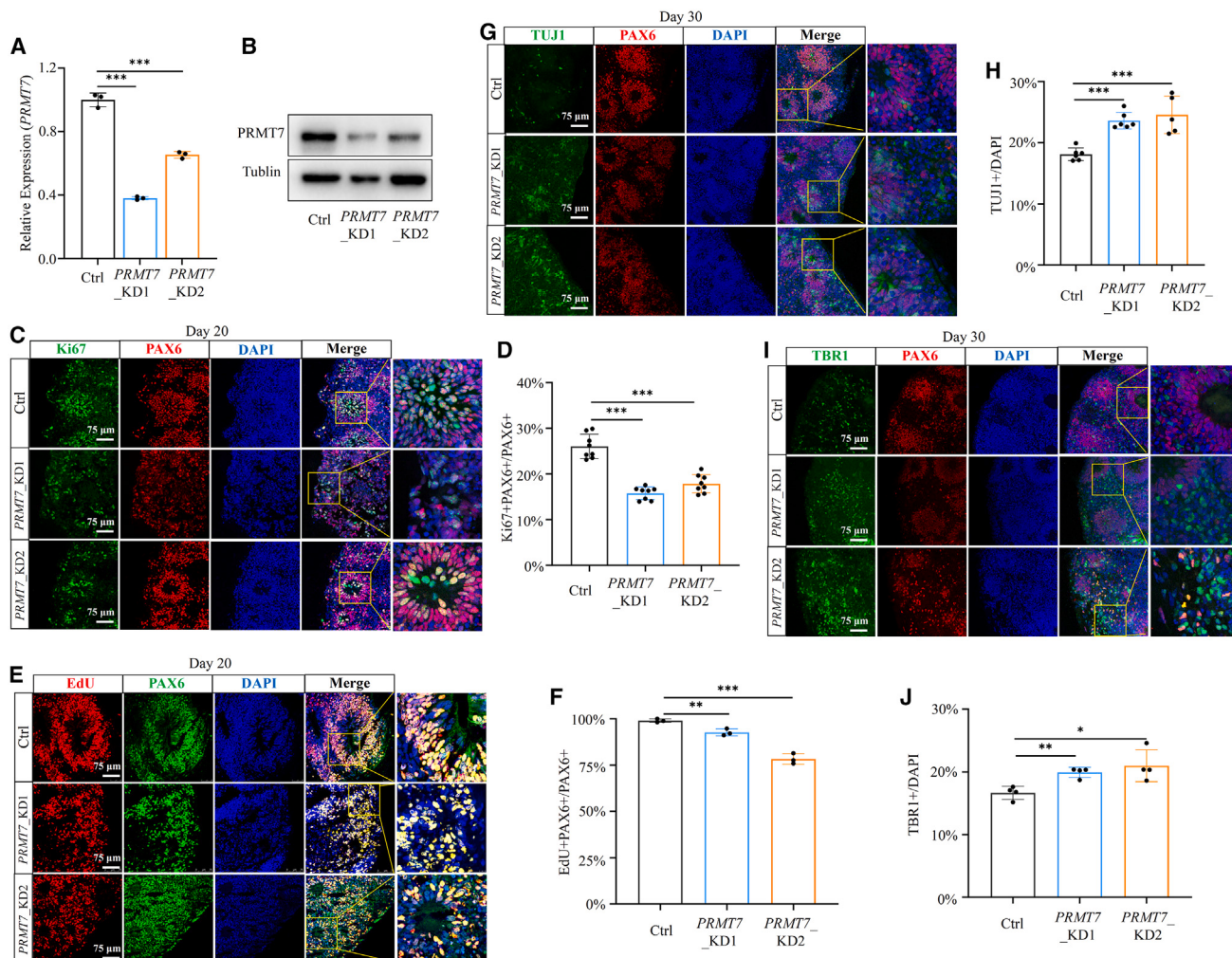


Figure 3. PRMT7 is involved in modulating NPC function in 3D cerebral organoids

(A and B) RT-qPCR (A) and western blot (B) for the detection of PRMT7 expression level in human embryonic stem cell line H9 with *PRMT7* knockdown or not. $p < 0.0001$ and $p = 0.0002$ in *PRMT7*_KD1 and *PRMT7*_KD2 compared to Ctrl, respectively. Values are expressed as mean \pm SD; $n = 3$ in (A). (C–F) Ki67 (C) and EdU (E) immunostaining for the proliferative cells in NPCs marked by PAX6 in *PRMT7*-downregulated cerebral organoids and the control and quantification of these cells by normalization to the PAX6-positive cells (D and F), respectively. The enlarged partial view of EdU or Ki67 and PAX6 co-staining is shown in the right of the merged picture of (C) and (E), respectively. $p < 0.0001$ in *PRMT7*_KD1 or *PRMT7*_KD2 compared to Ctrl, and values are expressed as mean \pm SD; $n = 8$ in (D). $p = 0.0059$ and $p = 0.0003$ in *PRMT7*_KD1 and *PRMT7*_KD2 compared to Ctrl, and values are expressed as mean \pm SD; $n = 3$ in (F). (G and I) TUJ1 (G) and TBR1 (I) immunostaining for the differentiated general neurons and the post-mitotic pyramidal neurons, respectively. (H and J) The occupancy of these cells is quantified by the number of total cells marked by DAPI. The right image shows an enlarged partial view of the merged picture. $p < 0.0001$ and $p = 0.0009$ in *PRMT7*_KD1 and *PRMT7*_KD2 compared to Ctrl, and values are expressed as mean \pm SD; $n = 6$ in (H). $p = 0.0026$ and $p = 0.0198$ in *PRMT7*_KD1 and *PRMT7*_KD2 compared to Ctrl, and values are expressed as mean \pm SD; $n = 4$ in (J).

* $p < 0.05$, ** $p < 0.01$, and *** $p < 0.001$ (two-sided Student's t test).

DISCUSSION

Several common genetic variants associated with SCZ susceptibility at 16q22.1 have been identified over the years, while their pathological mechanisms are still being uncovered. Through a comprehensive analysis of the published TWAS research, *cis*-eQTLs, and differential expression data, we speculated that *PRMT7* may be the functional gene at this locus. The following experimental exploration documented that *PRMT7* serves as the target of these SCZ-susceptible SNPs, supporting its contri-

bution to SCZ risk (Figure 1). Thus, this study confirmed at the genetic regulation level that *PRMT7* is tightly associated with SCZ.

Altered programmed neurodevelopmental trajectories are now accepted as a pathological mechanism of SCZ, including the impairments of NPC proliferation, neurogenesis, and neuronal outgrowth in early brain development.² It has been reported that *PRMT7* mutation leads to intellectual disability, implicating the involvement of *PRMT7* in neurodevelopment.^{19–21} However, there is little knowledge about how *PRMT7* regulates

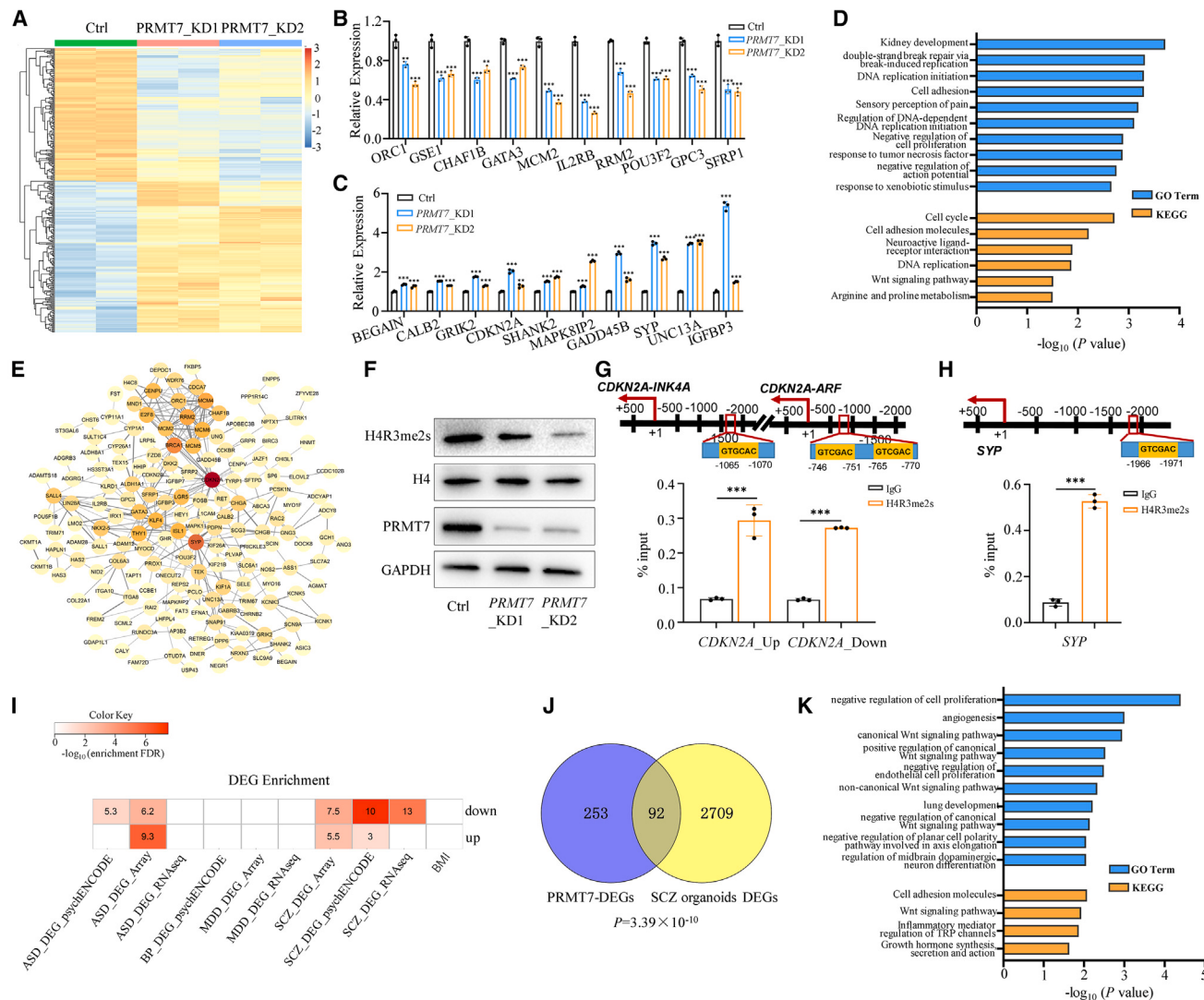


Figure 4. PRMT7-regulated DEGs are relevant to SCZ pathogenesis

(A) Heatmap for the DEGs by comparing the expression levels of the genes in *PRMT7*-knockdown NPCs to those in the control. (B and C) RT-qPCR validation for the randomly selected genes' expression (B, ORC1: $p = 0.0045$ and $p = 0.0004$; GSE1, $p = 0.0008$ and $p = 0.0013$; CHAF1B: $p = 0.0002$ and $p = 0.0010$; GATA3: $p < 0.0001$ and $p = 0.0002$; MCM2: $p = 0.0001$ and $p < 0.0001$; IL2RB: $p < 0.0001$ and $p < 0.0001$; RRM2: $p = 0.0001$ and $p < 0.0001$; POU3F2: $p < 0.0001$ and $p < 0.0001$; GPC3: $p = 0.0001$; and SFRP1: $p = 0.0003$ and $p = 0.0002$; C, BEGAIN: $p = 0.0003$ and $p = 0.0040$; CALB2, $p < 0.0001$ and $p < 0.0001$; GRIK2: $p < 0.0001$ and $p = 0.0002$; CDKN2A: $p = 0.0001$ and $p = 0.0071$; SHANK2: $p < 0.0001$ and $p < 0.0001$; MAPK8IP2: $p = 0.0002$ and $p < 0.0001$; GADD45B: $p < 0.0001$ and $p = 0.0005$; SYP: $p < 0.0001$ and $p < 0.0001$; UNC13A: $p < 0.0001$ and $p < 0.0001$; and IGFBP3: $p < 0.0001$ and $p = 0.0002$). Values are expressed as mean \pm SD; $n = 3$.

(D) Functional enrichment analysis of the overall DEGs.

(E) PPI network for the DEGs.

(F) Western blot for H4R3me2s and H4 in *PRMT7*-knockdown NPCs and the control cell.

(G and H) ChIP-qPCR for detecting the promoter regions containing CACGTG or CAGCTG of *CDKN2A* (G) and *SYP* (H) in ChIP and the input sample of H4R3me2s and immunoglobulin (IgG). $p = 0.0010$ for *CDKN2A*_Up, $p < 0.0001$ for *CDKN2A*_Down, and $p < 0.0001$ for *SYP* in H4R3me2s compared to IgG. Values are expressed as mean \pm SD; $n = 3$.

(I) The association of *PRMT7*-regulated DEGs with the DEGs in four neurodevelopmental disorders, including ASD, BP, MDD, and SCZ. Body mass index (BMI) acts as the internal control.

(J) Venn picture for the overlapped genes of *PRMT7*-regulated DEGs and SCZ organoid DEGs.

(K) Functional enrichment analysis of the shared genes in (J).

** $p < 0.01$ and *** $p < 0.001$ (two-sided Student's t test).

this process. In our study, we robustly demonstrated that PRMT7 controls NPC proliferation and differentiation into neurons when H9 or U1M cells were induced to develop cerebral organoids. It was detected that *PRMT7* downregulation contributed to the decreased proliferation of NPCs, while its differentiation into neurons was significantly increased (Figures 3 and S14). The functional enrichment offered further molecular evidence that PRMT7-regulated DEGs were predominantly associated with the cell cycle, such as *CDKN2A*, encoding a significant regulator of the G1-to-S phase transition (Figure 4D). Additionally, we found that Wnt signaling also showed significant enrichment in PRMT7-regulated DEGs, particularly in the shared genes of these DEGs and SCZ-associated genes (Figures 4D and 4K). It is well known that the Wnt pathway is crucial for brain development and that its dysfunction is closely associated with many mental disorders, including SCZ, BD, and ASD.^{23–25} One potential mechanism linking it to these illness may be its aberrant regulation on NPC proliferation and differentiation.^{24,26} Furthermore, the genes, showing differentially expressed-upon PRMT7 upregulation, were also related to cell proliferation signaling, such as the DNA damage response, through analysis of *PRMT7*-overexpressed RNA-seq data (Figures S8J–S8L). Therefore, *PRMT7* dysregulation on NPC function during neurodevelopment may explain, at least in part, the contribution of PRMT7 to SCZ risk.

PRMT7 also plays a key role in regulating neuron function.^{27,28} The mice with *PRMT7* deficiency displayed neuronal hyperexcitability and abnormal social behavior.^{27,28} In this study, we found that the differentiated neurons displayed impaired morphological development, featured by elongated neurites, when *PRMT7* was downregulated (Figures 2F–2H). Additionally, the RNA-seq result showed that PRMT7 may also regulate neuronal function (Figure 4D). For example, some of the PRMT7-regulated DEGs were significantly enriched in the cell adhesion molecules and neuron-activity-related pathways, including negative regulation of action potential and neuroactive ligand-receptor interaction. Cell adhesion molecules are well known to be significant regulators in neuronal axon growth and guidance and synapse formation and maturation.²⁹ Emerging evidence has implicated the involvement of cell adhesion molecules in SCZ pathogenesis.^{30,31} The deletions or mutations of neuroligins and neurexins, two kinds of well-characterized cell adhesion molecules, have been found in patients with SCZ, and these variants commonly led to impaired synapse structure and function.^{30,31} Thus, the regulatory role of PRMT7 in cell adhesion molecules and its effect on synapse morphology and neuronal activity deserve to be explored in future investigations.

It has been known that PRMT7 modulates gene expression by impacting the modification level of H4R3me2s, a repressive chromatin mark, as an epigenetic regulator.^{22,32,33} Here, the two hub genes *CDKN2A* and *SYP*, individually related to the cell cycle and neuron function, were examined to have an H4R3me2s modification on their promoter region. Upon *PRMT7* knockdown, the overall H4R3me2s level was decreased, and these two genes' expression was increased, indicating that they may be the direct targets of PRMT7. Whether there are other direct downstream effectors of PRMT7 among the DEGs needs to be further uncovered. Besides, many non-histone proteins associated with RNA splicing, transportation, and stabilization

have been identified to be the substrates of PRMT7 through arginine methylome profiling.^{34,35} In breast cancer cells, PRMT7 upregulation led to aberrant alternative splicing through methylating the splicing factor hnRNPA1, consequently increasing cell growth.³⁴ Therefore, we can also investigate whether PRMT7 can methylate non-histone proteins to regulate NPC proliferation and differentiation in the future.

In conclusion, in this study, we first provided evidence that *PRMT7* may act as a functional gene linking the SNPs at 16q22.1 to SCZ susceptibility. Then, we unveiled the mechanism from the cellular to molecular level that *PRMT7* dysregulation contributes to SCZ risk, possibly due to the disruption of NPC proliferation and neuronal differentiation. Hence, this study opens a mechanistic insight into understanding the etiology of the genetic factor contributing to SCZ risk at 16q22.1.

Limitations of the study

In this study, *cis*-eQTL analysis and publicly available chromosome conformation capture data suggested that SCZ risk SNPs at 16q22.1 may regulate PRMT7 expression. We then provided experimental evidence that PRMT7 is indeed a downstream target of these SNPs by performing a dual-luciferase assay followed by CRISPR-dCas9. Here, another effective approach to confirm the regulation of the SNPs on PRMT7 expression is to introduce a specific allele at these SNP loci through homologous recombination (HR) using CRISPR-Cas9 or the single base editor. To further elucidate the relationship between PRMT7 and these SCZ risk SNPs, future studies could apply this experiment to establish the cell line carrying the different alleles of these SNPs.

RESOURCE AVAILABILITY

Lead contact

Requests for further information and for resources and reagents should be directed to and will be fulfilled by the lead contact, Chao Chen (chenchao@sklmg.edu.cn).

Materials availability

This study did not generate unique reagents.

Data and code availability

- RNA-seq data generated in this study are available at the Gene Expression Omnibus (GEO). The accession numbers are listed in the [key resources table](#).
- All code used in this study has been previously published, and the analysis pipelines are described in the [STAR Methods](#).
- Any additional information required to reanalyze the data reported in this paper is available from the lead contact upon request.

ACKNOWLEDGMENTS

This work is supported by the National Key Research and Development Program of China (no. 2024YFA1108000), the National Natural Science Foundation of China (no. 82022024), the Natural Science Foundation of Hunan Province (no. 2023JJ40789), and the Science and Technology Innovation Program of Hunan Province (nos. 2021RC4018 and 2021RC5027). We acknowledge the computing resources provided by the High-Performance Computing Center of Central South University and the Bioinformatics Center of Furong Laboratory.

AUTHOR CONTRIBUTIONS

C.C. and T.S. conceived the overall project and supervised its execution. T.S. performed data integration and interpretation and drafted the manuscript. C.C., C.L., and K.L. revised the manuscript. J.Y. and B.X. contributed to the functional experiments. C.H. and J.C. performed the data analysis. All authors have reviewed and approved the final paper.

DECLARATION OF INTERESTS

The authors declare no competing interests.

STAR★METHODS

Detailed methods are provided in the online version of this paper and include the following:

- **KEY RESOURCES TABLE**
- **EXPERIMENTAL MODEL AND STUDY PARTICIPANT DETAILS**
 - Cell lines
- **METHOD DETAILS**
 - Generation of neural progenitor cells
 - Dual-luciferase reporter assay
 - CRISPR-dCas9
 - Lentivirus infection
 - Generation of 2D forebrain neurons
 - Generation of 3D cerebral organoids
 - RNA and protein extraction, RT-qPCR, and western blot
 - NPCs proliferation assay
 - Immunocytochemistry
 - RNA-seq and data analysis
 - Protein-protein interaction network analysis
 - Chromatin immunoprecipitation
- **QUANTIFICATION AND STATISTICAL ANALYSIS**

SUPPLEMENTAL INFORMATION

Supplemental information can be found online at <https://doi.org/10.1016/j.celrep.2025.115279>.

Received: June 5, 2024

Revised: November 22, 2024

Accepted: January 16, 2025

Published: February 6, 2025

REFERENCES

1. Guan, F., Ni, T., Zhu, W., Williams, L.K., Cui, L.-B., Li, M., Tubbs, J., Sham, P.-C., and Gui, H. (2022). Integrative omics of schizophrenia: from genetic determinants to clinical classification and risk prediction. *Mol. Psychiatr.* 27, 113–126. <https://doi.org/10.1038/s41380-021-01201-2>.
2. Birnbaum, R., and Weinberger, D.R. (2017). Genetic insights into the neurodevelopmental origins of schizophrenia. *Nat. Rev. Neurosci.* 18, 727–740. <https://doi.org/10.1038/nrn.2017.125>.
3. Zeng, B., Bendl, J., Kosoy, R., Fullard, J.F., Hoffman, G.E., and Roussos, P. (2022). Multi-ancestry eQTL meta-analysis of human brain identifies candidate causal variants for brain-related traits. *Nat. Genet.* 54, 161–169. <https://doi.org/10.1038/s41588-021-00987-9>.
4. Zhang, W., Zhang, M., Xu, Z., Yan, H., Wang, H., Jiang, J., Wan, J., Tang, B., Liu, C., Chen, C., and Meng, Q. (2023). Human forebrain organoid-based multi-omics analyses of PCCB as a schizophrenia associated gene linked to GABAergic pathways. *Nat. Commun.* 14, 5176. <https://doi.org/10.1038/s41467-023-40861-2>.
5. Dong, P., Voloudakis, G., Fullard, J.F., Hoffman, G.E., and Roussos, P. (2024). Convergence of the dysregulated regulome in schizophrenia with polygenic risk and evolutionarily constrained enhancers. *Mol. Psychiatr.* 29, 782–792. <https://doi.org/10.1038/s41380-023-02370-y>.
6. Mai, J., Lu, M., Gao, Q., Zeng, J., and Xiao, J. (2023). Transcriptome-wide association studies: recent advances in methods, applications and available databases. *Commun. Biol.* 6, 899. <https://doi.org/10.1038/s42003-023-05279-y>.
7. Gandal, M.J., Zhang, P., Hadjimichael, E., Walker, R.L., Chen, C., Liu, S., Won, H., van Bakel, H., Varghese, M., Wang, Y., et al. (2018). Transcriptome-wide isoform-level dysregulation in ASD, schizophrenia, and bipolar disorder. *Science* 362, eaat8127. <https://doi.org/10.1126/science.aat8127>.
8. Gusev, A., Mancuso, N., Won, H., Kousi, M., Finucane, H.K., Reshef, Y., Song, L., Safi, A., Schizophrenia Working Group of the Psychiatric Genomics Consortium; McCarroll, S., and Neale, B.M. (2018). Transcriptome-wide association study of schizophrenia and chromatin activity yields mechanistic disease insights. *Nat. Genet.* 50, 538–548. <https://doi.org/10.1038/s41588-018-0092-1>.
9. Huckins, L.M., Dobryn, A., Ruderfer, D.M., Hoffman, G., Wang, W., Pardiñas, A.F., Rajagopal, V.M., Als, T.D., T Nguyen, H., Girdhar, K., et al. (2019). Gene expression imputation across multiple brain regions provides insights into schizophrenia risk. *Nat. Genet.* 51, 659–674. <https://doi.org/10.1038/s41588-019-0364-4>.
10. Hall, L.S., Medway, C.W., Pain, O., Pardiñas, A.F., Rees, E.G., Escott-Price, V., Pocklington, A., Bray, N.J., Holmans, P.A., Walters, J.T.R., et al. (2020). A transcriptome-wide association study implicates specific pre- and post-synaptic abnormalities in schizophrenia. *Hum. Mol. Genet.* 29, 159–167. <https://doi.org/10.1093/hmg/ddz253>.
11. Liu, J., Li, S., Li, X., Li, W., Yang, Y., Guo, S., Lv, L., Xiao, X., Yao, Y.-G., Guan, F., et al. (2021). Genome-wide association study followed by trans-ancestry meta-analysis identify 17 new risk loci for schizophrenia. *BMC Med.* 19, 177. <https://doi.org/10.1186/s12916-021-02039-9>.
12. Fiorica, P.N., and Wheeler, H.E. (2019). Transcriptome association studies of neuropsychiatric traits in African Americans implicate PRMT7 in schizophrenia. *PeerJ* 7, e7778. <https://doi.org/10.7717/peerj.7778>.
13. (2014). Biological insights from 108 schizophrenia-associated genetic loci. *Nature* 511, 421–427. <https://doi.org/10.1038/nature13595>.
14. Pardiñas, A.F., Holmans, P., Pocklington, A.J., Escott-Price, V., Ripke, S., Carrera, N., Legge, S.E., Bishop, S., Cameron, D., Hamshere, M.L., et al. (2018). Common schizophrenia alleles are enriched in mutation-intolerant genes and in regions under strong background selection. *Nat. Genet.* 50, 381–389. <https://doi.org/10.1038/s41588-018-0059-2>.
15. Smeland, O.B., Bahrami, S., Frei, O., Shadrin, A., O'Connell, K., Savage, J., Watanabe, K., Krull, F., Bettella, F., Steen, N.E., et al. (2020). Genome-wide analysis reveals extensive genetic overlap between schizophrenia, bipolar disorder, and intelligence. *Mol. Psychiatr.* 25, 844–853. <https://doi.org/10.1038/s41380-018-0332-x>.
16. Lam, M., Hill, W.D., Trampush, J.W., Yu, J., Knowles, E., Davies, G., Stahl, E., Huckins, L., Liewald, D.C., Djurovic, S., et al. (2019). Pleiotropic Meta-Analysis of Cognition, Education, and Schizophrenia Differentiates Roles of Early Neurodevelopmental and Adult Synaptic Pathways. *Am. J. Hum. Genet.* 105, 334–350. <https://doi.org/10.1016/j.ajhg.2019.06.012>.
17. Trubetskoy, V., Pardiñas, A.F., Qi, T., Panagiotaropoulou, G., Awasthi, S., Bigdeli, T.B., Bryois, J., Chen, C.Y., Dennison, C.A., Hall, L.S., et al. (2022). Mapping genomic loci implicates genes and synaptic biology in schizophrenia. *Nature* 604, 502–508. <https://doi.org/10.1038/s41586-022-04434-5>.
18. Jiao, C., Yan, P., Xia, C., Shen, Z., Tan, Z., Tan, Y., Wang, K., Jiang, Y., Huang, L., Dai, R., et al. (2019). BrainEXP: a database featuring with spatiotemporal expression variations and co-expression organizations in human brains. *Bioinformatics* 35, 172–174. <https://doi.org/10.1093/bioinformatics/bty576>.
19. Agolini, E., Dentici, M.L., Bellacchio, E., Alesi, V., Radio, F.C., Torella, A., Musacchia, F., Tartaglia, M., Dallapiccola, B., Nigro, V., et al. (2018). Expanding the clinical and molecular spectrum of PRMT7 mutations: 3

- additional patients and review. *Clin. Genet.* 93, 675–681. <https://doi.org/10.1111/cge.13137>.
20. Kernohan, K.D., McBride, A., Xi, Y., Martin, N., Schwartzenbuber, J., Dymment, D.A., Majewski, J., Blaser, S., Care4Rare Canada Consortium; Boycott, K.M., and Chitayat, D. (2017). Loss of the arginine methyltransferase PRMT7 causes syndromic intellectual disability with microcephaly and brachydactyly. *Clin. Genet.* 97, 708–716. <https://doi.org/10.1111/cge.12884>.
 21. Akawi, N., McRae, J., Ansari, M., Balasubramanian, M., Blyth, M., Brady, A.F., Clayton, S., Cole, T., Deshpande, C., Fitzgerald, T.W., et al. (2015). Discovery of four recessive developmental disorders using probabilistic genotype and phenotype matching among 4,125 families. *Nat. Genet.* 47, 1363–1369. <https://doi.org/10.1038/ng.3410>.
 22. Jain, K., Jin, C.Y., and Clarke, S.G. (2017). Epigenetic control via allosteric regulation of mammalian protein arginine methyltransferases. *Proc. Natl. Acad. Sci. USA* 114, 10101–10106. <https://doi.org/10.1073/pnas.1706978114>.
 23. Hoseth, E.Z., Krull, F., Dieset, I., Mørch, R.H., Hope, S., Gardsjord, E.S., Steen, N.E., Melle, I., Brattbakk, H.-R., Steen, V.M., et al. (2018). Exploring the Wnt signaling pathway in schizophrenia and bipolar disorder. *Transl. Psychiatry* 8, 55. <https://doi.org/10.1038/s41398-018-0102-1>.
 24. Gao, J., Liao, Y., Qiu, M., and Shen, W. (2021). Wnt/β-Catenin Signaling in Neural Stem Cell Homeostasis and Neurological Diseases. *Neuroscientist* 27, 58–72. <https://doi.org/10.1177/1073858420914509>.
 25. Jiang, C.-C., Lin, L.-S., Long, S., Ke, X.-Y., Fukunaga, K., Lu, Y.-M., and Han, F. (2022). Signalling pathways in autism spectrum disorder: mechanisms and therapeutic implications. *Signal Transduct. Targeted Ther.* 7, 229. <https://doi.org/10.1038/s41392-022-01081-0>.
 26. Mulligan, K.A., and Cheyette, B.N.R. (2017). Neurodevelopmental Perspectives on Wnt Signaling in Psychiatry. *Complex Psychiatry* 2, 219–246. <https://doi.org/10.1159/000453266>.
 27. Lee, S.Y., Vuong, T.A., Wen, X., Jeong, H.J., So, H.K., Kwon, I., Kang, J.S., and Cho, H. (2019). Methylation determines the extracellular calcium sensitivity of the leak channel NALCN in hippocampal dentate granule cells. *Exp. Mol. Med.* 51, 1–14. <https://doi.org/10.1038/s12276-019-0325-0>.
 28. Lee, S.Y., Vuong, T.A., So, H.K., Kim, H.J., Kim, Y.B., Kang, J.S., Kwon, I., and Cho, H. (2020). PRMT7 deficiency causes dysregulation of the HCN channels in the CA1 pyramidal cells and impairment of social behaviors. *Exp. Mol. Med.* 52, 604–614. <https://doi.org/10.1038/s12276-020-0417-x>.
 29. Sakurai, T. (2017). The role of cell adhesion molecules in brain wiring and neuropsychiatric disorders. *Mol. Cell. Neurosci.* 81, 4–11. <https://doi.org/10.1016/j.mcn.2016.08.005>.
 30. Tromp, A., Mowry, B., and Giacometto, J. (2021). Neurexins in autism and schizophrenia—a review of patient mutations, mouse models and potential future directions. *Mol. Psychiatr.* 26, 747–760. <https://doi.org/10.1038/s41380-020-00944-8>.
 31. Liu, X., Hua, F., Yang, D., Lin, Y., Zhang, L., Ying, J., Sheng, H., and Wang, X. (2022). Roles of neuroligins in central nervous system development: focus on glial neuroligins and neuron neuroligins. *J. Transl. Med.* 20, 418. <https://doi.org/10.1186/s12967-022-03625-y>.
 32. Blanc, R.S., Vogel, G., Chen, T., Crist, C., and Richard, S. (2016). PRMT7 Preserves Satellite Cell Regenerative Capacity. *Cell Rep.* 14, 1528–1539. <https://doi.org/10.1016/j.celrep.2016.01.022>.
 33. Shen, T., Ni, T., Chen, J., Chen, H., Ma, X., Cao, G., Wu, T., Xie, H., Zhou, B., Wei, G., et al. (2022). An enhancer variant at 16q22.1 predisposes to hepatocellular carcinoma via regulating PRMT7 expression. *Nat. Commun.* 13, 1232. <https://doi.org/10.1038/s41467-022-28861-0>.
 34. Li, W.J., He, Y.H., Yang, J.J., Hu, G.S., Lin, Y.A., Ran, T., Peng, B.L., Xie, B.L., Huang, M.F., Gao, X., et al. (2021). Profiling PRMT methylome reveals roles of hnRNPA1 arginine methylation in RNA splicing and cell growth. *Nat. Commun.* 12, 1946. <https://doi.org/10.1038/s41467-021-21963-1>.
 35. Szewczyk, M.M., Ishikawa, Y., Organ, S., Sakai, N., Li, F., Halabelian, L., Ackloo, S., Couzens, A.L., Eram, M., Dilworth, D., et al. (2020). Pharmacological inhibition of PRMT7 links arginine monomethylation to the cellular stress response. *Nat. Commun.* 11, 2396. <https://doi.org/10.1038/s41467-020-16271-z>.
 36. Martin, M. (2011). Cutadapt removes adapter sequences from high-throughput sequencing reads. *EMBnet J.* 17, 10–12. <https://doi.org/10.14806/EJ.17.1.200>.
 37. Dobin, A., Davis, C.A., Schlesinger, F., Drenkow, J., Zaleski, C., Jha, S., Batut, P., Chaisson, M., and Gingeras, T.R. (2013). STAR: ultrafast universal RNA-seq aligner. *Bioinformatics* 29, 15–21. <https://doi.org/10.1093/bioinformatics/bts635>.
 38. Patro, R., Duggal, G., Love, M.I., Irizarry, R.A., and Kingsford, C. (2017). Salmon provides fast and bias-aware quantification of transcript expression. *Nat. Methods* 14, 417–419. <https://doi.org/10.1038/nmeth.4197>.
 39. Law, C.W., Chen, Y., Shi, W., and Smyth, G.K. (2014). voom: Precision weights unlock linear model analysis tools for RNA-seq read counts. *Genome Biol.* 15, R29. <https://doi.org/10.1186/gb-2014-15-2-r29>.
 40. Sherman, B.T., Hao, M., Qiu, J., Jiao, X., Baseler, M.W., Lane, H.C., Ima-michi, T., and Chang, W. (2022). DAVID: a web server for functional enrichment analysis and functional annotation of gene lists (2021 update). *Nucleic Acids Res.* 50, W216–W221. <https://doi.org/10.1093/nar/gkac194>.
 41. Zhou, Y., Zhou, B., Pache, L., Chang, M., Khodabakhshi, A.H., Tanaseichuk, O., Benner, C., and Chanda, S.K. (2019). Metascape provides a biologist-oriented resource for the analysis of systems-level datasets. *Nat. Commun.* 10, 1523. <https://doi.org/10.1038/s41467-019-09234-6>.
 42. Szklarczyk, D., Kirsch, R., Koutrouli, M., Nastou, K., Mehryary, F., Hachilif, R., Gable, A.L., Fang, T., Doncheva, N.T., Pyysalo, S., et al. (2023). The STRING database in 2023: protein–protein association networks and functional enrichment analyses for any sequenced genome of interest. *Nucleic Acids Res.* 51, D638–D646. <https://doi.org/10.1093/nar/gkac1000>.
 43. Shannon, P., Markiel, A., Ozier, O., Baliga, N.S., Wang, J.T., Ramage, D., Amin, N., Schwikowski, B., and Ideker, T. (2003). Cytoscape: A Software Environment for Integrated Models of Biomolecular Interaction Networks. *Genome Res.* 13, 2498–2504. <https://doi.org/10.1101/gr.123903>.
 44. Ongen, H., Buil, A., Brown, A.A., Dermizakis, E.T., and Delaneau, O. (2016). Fast and efficient QTL mapper for thousands of molecular phenotypes. *Bioinformatics* 32, 1479–1485. <https://doi.org/10.1093/bioinformatics/btv722>.
 45. Shabalin, A.A. (2012). Matrix eQTL: ultra fast eQTL analysis via large matrix operations. *Bioinformatics* 28, 1353–1358. <https://doi.org/10.1093/bioinformatics/bts163>.

STAR★METHODS

KEY RESOURCES TABLE

REAGENT or RESOURCE	SOURCE	IDENTIFIER
Antibodies		
secondary antibody anti-Rabbit IgG	Jackson Immune Research	Cat# 711035152; RRID: AB_10015282
secondary antibody anti-Mouse IgG	Jackson Immune Research	Cat# 715035150; RRID: AB_2340770
rabbit anti-PRMT7	Abcam	Cat# ab181214
rabbit anti-H4	Abcam	Cat# ab177840; RRID: AB_2650469
rabbit anti-NESTIN	Abcam	Cat# ab105389; RRID: AB_10859398
mouse anti-PAX6	Abcam	Cat# ab78545; RRID: AB_1566562
rabbit anti-H4R3me2s	Active motif	Cat# 61187; RRID: AB_2793544
rabbit anti-GAPDH	AntGene	Cat# ANT325; RRID: AB_2905629
mouse anti-tubulin	sigma-Aldrich	Cat# T6199; RRID: AB_477583
rabbit anti-MMA	Cell Signaling Technology	Cat# 8015; RRID: AB_10891776
rabbit anti-SOX2	Cell Signaling Technologies	Cat# 3579S; RRID: AB_2195767
mouse anti-TRA-1-60	Cell Signaling Technologies	Cat# 4746S; RRID: AB_2119059
mouse anti-SSEA4	Cell Signaling Technologies	Cat# 4755S; RRID: AB_1264259
rabbit anti-OCT4	Cell Signaling Technologies	Cat# 2750S; RRID: AB_823583
rabbit anti-PAX6	Cell Signaling Technologies	Cat# 60433S; RRID: AB_2797599
mouse anti-ki67	Cell Signaling Technologies	Cat# 9449S; RRID: AB_2797703
rabbit anti-TUJ1	Cell Signaling Technologies	Cat# 5568S; RRID: AB_10694505
mouse anti-TUJ1	Cell Signaling Technologies	Cat# 4466S; RRID: AB_1904176
rabbit anti-TBR1	Cell Signaling Technologies	Cat# 49661S; RRID: AB_2799364
rabbit anti-GFAP	GeneTEX	Cat# GTX108711; RRID: AB_2037091
Chemicals, peptides, and recombinant proteins		
Matrigel	Corning	Cat# 354277
penicillin-streptomycin	Gibco	Cat# 10378016
DMEM	Gibco	Cat# C11995500BT
fetal bovine serum	Gibco	Cat# A3161001C
mTeSR Plus medium	STEMCELL Technologies	Cat# 100-0276
Neural Induction Medium	STEMCELL Technologies	Cat# 05835
Anti-Adherence Rinsing Solution	STEMCELL Technologies	Cat# 7010
Y-27632	STEMCELL Technologies	Cat# 2307
Neural Rosette Selection Reagent	STEMCELL Technologies	Cat# 05832
Neural Progenitor Medium	STEMCELL Technologies	Cat# 05833
Neuron Differentiation and Maturation Kit	STEMCELL Technologies	Cat# 08600, 08605
Cerebral Organoid Kit	STEMCELL Technologies	Cat# 08570, 08571
endotoxin-free plasmid extraction kit	Omega	Cat# M6399-00S
Lipofectamine 3000	Thermo Fisher	Cat# L3000015
Poly-L-ornithine hydrobromide	SIGMA	Cat# P3655
Laminin	SIGMA	Cat# 11243217001
TRIzol Reagent	Invitrogen	Cat# 10296010
HiScript®III RT SuperMix of qPCR Kit	Vazyme	Cat# R323-01
2×SYBR mix	Vazyme	Cat# R711-02
SDS-PAGE gels	Solarbio	Cat# P1200
1X TBST	Yamei	Cat# PS103S
cell counting kit-8	Beyotime	Cat# C0038

(Continued on next page)

Continued

REAGENT or RESOURCE	SOURCE	IDENTIFIER
BeyoClic EdU-555 cell proliferation kit	Beyotime	Cat# C0075L
DAPI	Beyotime	Cat# C1002
embedding agent	SAKURA	Cat# 4583
Dual Luciferase Reporter Assay System	Promega	Cat# E1960
TruSeq Stranded Total RNA kit	Illumina	Cat# RS-122-2301
SimpleChIP® Enzymatic Chromatin IP Kit	Cell Signaling Technologies	Cat# 9003
Critical consumables		
AggreWell 800 24-well plate	STEMCELL Technologies	Cat# 34815
ultra-low attachment 96-well plate	Corning	Cat# 7007
ultra-low attachment 24-well plate	Corning	Cat# 3473
ultra-low attachment 6-well plate	Corning	Cat# 3471
cold wet transfer apparatus	BIO-RAD	Cat# 1658004
coverslips	JingAn Biological	Cat# J12001
specimen molds	SAKURA	Cat# 4565
ImmEdge® Pen	VECTOR	Cat# H-4000
Experimental models: cell lines		
H9 cells	ATCC	–
U1M cells	ATCC	–
SH-SY5Y cells	ATCC	–
Software and algorithms		
ImageJ	National Institutes of Health	https://imagej.net/ij/
GraphPad Prism 10	GraphPad	https://www.graphpad.com/
FastQC	–	https://www.bioinformatics.babraham.ac.uk/
cutadapt	Martin et al. ³⁶	https://github.com/marcelm/cutadapt/
STAR	Dobin et al. ³⁷	https://github.com/alexdobin/STAR/
salmon	Patro et al. ³⁸	https://github.com/COMBINE-lab/Salmon/
Limma-voom	Law et al. ³⁹	https://bioinf.wehi.edu.au/voom/
DAVID	Sherman et al. ⁴⁰	https://davidbioinformatics.nih.gov/
Metascape	Zhou et al. ⁴¹	https://www.metascape.org/
STRING	Szklarczyk et al. ⁴²	https://cn.string-db.org/
Cytoscape	Shannon et al. ⁴³	https://cytoscape.org/
Oligonucleotides		
qPCR primers, gRNAs, and shRNAs, see Table S6	–	–
Recombinant DNA		
pGL3-Promoter-Enhancer A (rs1975802)	This paper	–
pGL3-Promoter-Enhancer G (rs1975802)	This paper	–
pGL3-Promoter-Enhancer C (rs11861362)	This paper	–
pGL3-Promoter-Enhancer G (rs11861362)	This paper	–
pGL3-PRMT7 Promoter-Enhancer A (rs1975802)	This paper	–
pGL3-PRMT7 Promoter-Enhancer G (rs1975802)	This paper	–
pGL3-PRMT7 Promoter-Enhancer C (rs11861362)	This paper	–
pGL3-PRMT7 Promoter-Enhancer G (rs11861362)	This paper	–
PBC2-dCa9-KRAB-gRNA targeting rs1975802-containing region	This paper	–
PBC2-dCa9-KRAB-gRNA targeting rs11861362-containing region	This paper	–
PBC2-dCa9-VP48-gRNA targeting rs1975802-containing region	This paper	–

(Continued on next page)

Continued

REAGENT or RESOURCE	SOURCE	IDENTIFIER
PBC2-dCas9-VP48-gRNA targeting rs11861362-containing region	This paper	—
VP013-U6-MCS-CMV-ZsGreen-PGK-PURO-PRMT7-sh1	This paper	—
VP013-U6-MCS-CMV-ZsGreen-PGK-PURO-PRMT7-sh2	This paper	—
pLV2itr-EGFP-Puro-EF1 α -PRMT7	This paper	—
Deposited data		
RNA-seq	Raw data and gene expression counts	GEO: GSE266062, GSE284672

EXPERIMENTAL MODEL AND STUDY PARTICIPANT DETAILS

Cell lines

The H9 embryonic stem cells (ESCs), U1M iPSCs, and SH-SY5Y neuroblastoma cells are originally obtained from American Type Culture Collection (ATCC, <https://www.atcc.org>). The stem-ness and pluripotency for H9 and U1M have been confirmed via immunostaining of OCT4 and SOX2, TRA-1-60 and SSEA4, respectively. The karyotype analysis shows the normal and complete composition of chromosomes in H9 and U1M. SH-SY5Y has been authenticated by short tandem repeat (STR) assay. Additionally, these three cell lines do not have mycoplasma contamination. H9 and U1M are cultured with mTeSR Plus medium (STEMCELL Technologies) supplemented with 1% penicillin-streptomycin (Gibco) in the 12-well plate coated with Matrigel (Corning). SH-SY5Y are cultured in the high-glucose DMEM (Gibco) supplemented with 10% fetal bovine serum (Gibco) and 1% penicillin-streptomycin. All cells are cultured at 37°C in an incubator with 5% CO₂.

METHOD DETAILS

Generation of neural progenitor cells

H9 ESCs are differentiated into NPCs using Neural Induction Medium (STEMCELL Technologies). In brief, ESCs are dissociated into single cells using Accutase at day 0. 3 × 10⁶ cells are seeded into an AggreWell 800 24-well plate (STEMCELL Technologies) that has been treated with Anti-Adherence Rinsing Solution (STEMCELL Technologies), and then cultured with 1 mL Neural Induction Medium supplemented with 10 μM Y-27632 (STEMCELL Technologies). The next day, the embryoid bodies (EBs) are formed and cultured with 1 mL fresh Neural Induction Medium but without Y27632 from this day to day 4. At day 5, the EBs are transferred to a Matrigel-coated 6-well plate and the Neural Induction Medium is replaced every day. At day 12, neural rosettes are selected by using Neural Rosette Selection Reagent (STEMCELL Technologies), and then seeded into a new Matrigel-coated 6-well plate. The Neural Induction Medium is continuously changed every day for 5 days. Until day 17, the NPCs are formed and cultured in Neural Progenitor Medium (STEMCELL Technologies).

Dual-luciferase reporter assay

Firstly, the DNA sequence containing each allele of rs1975802 (hg19, chr16:68285780-68285917) or rs11861362 (hg19, chr16:68418729-68418859) is inserted into the pGL3-promotor plasmid or pGL3 basic plasmid with PRMT7 promoter (hg19, chr16:68344636-68345123). The positive clones are selected and then extended culture for the plasmid extraction using an endo-toxin-free plasmid extraction kit (Omega). Subsequently, the plasmid with the insertion of target DNA sequence or the empty vector plus the pRLTK, serving as an internal reference, is separately transferred into cells seeded in the 24-well plate using Lipofectamine 3000 (Thermo Fisher). After 24 h of transfection, the Firefly and Renilla luciferase activities are successively measured following the manufacturer's instruction (Promega). The final luciferase activity is through normalization of Firefly luciferase value to the Renilla.

CRISPR-dCas9

The gRNAs targeting the surrounding regions of rs1975802 or rs11861362 are designed at the zlab Guide Design website (<http://chopchop.cbu.uib.no/>). Then they are individually cloned into the plasmid containing dCas9 coupled with the suppressive domain KRAB (dCas9i) or the active domain VP48 (dCas9a). Subsequently, the plasmid containing the gRNA or the control vector plus pBase is transferred into cells in the 6-well plate using Lipofectamine 3000. The positive cells are selected using hygromycin at least for 7 days (400 μg/mL) post 24 h of transfection, and the culture medium is needed to be replaced every day for the removal of dead cells. After this procedure, the survival cells are maintained in the medium with low concentration of hygromycin till the large population. Finally, these cells are passaged for preservation or are used to extract RNA for the measurement of the PRMT7 expression level. The gRNA sequences are listed in [Table S6](#).

Lentivirus infection

The lentiviral particles containing shRNA (shRNA1 or shRNA3) vector targeting *PRMT7* are transduced into H9 ESCs and NPCs, respectively. Cells are infected with the lentiviruses for 24 h, and then cultured with fresh medium. At 72 h, cells with the integration of shRNA into genome are selected by medium with puromycin (1 µg/mL) for 3–7 days. The knockdown efficiency is confirmed by RT-qPCR and western blot. The shRNA sequences can be found in [Table S6](#).

Generation of 2D forebrain neurons

Neuronal differentiation is induced by Forebrain Neuron Differentiation and Maturation Kit (STEMCELL Technologies). At day 0, 6×10^5 NPCs are seeded into a 6-well plate that has been treated with Poly-L-ornithine hydrobromide (PLO) (15 µg/mL, SIGMA) and Laminin (5 µg/mL, SIGMA) and cultured in Neural Progenitor Medium. Next day, cells are cultured in Forebrain Neuron Differentiation Medium with daily change for 6 days. At day 7, 2×10^5 cells are transferred to a new 6-well plate that is treated with PLO and Laminin, and cultured in Forebrain Neuron Maturation Medium. The culture medium is replaced every two or three days and for at least 8 days.

Generation of 3D cerebral organoids

The H9 ESCs with *PRMT7* knockdown and the control cells are individually induced to generate 3D cerebral organoids using the Cerebral Organoid Kit (STEMCELL Technologies). Briefly, ESCs are dissociated into single cells using Accutase at day 0. 9×10^3 cells per well are seeded in an ultra-low attachment 96-well plate (Corning) with EB formation medium containing 10 µM Y-27632. At day 2 and day 4, each well is gently added with 100 µL EB formation medium without Y27632. At day 5, the EBs are transferred to an ultra-low attachment 24-well plate (Corning) and cultured in neural induction medium. At day 7, the EBs are embedded in Matrigel and incubated for 30 min at 37°C, and then are transferred to an ultra-low attachment 6-well plate (Corning) with neural expansion medium. At day 10, this 6-well plate is placed on an orbital shaker at a speed set of 70–80 rpm. Finally, the EBs are cultured in the maturation medium for at least 30 days and with a full medium change every 3–4 days.

RNA and protein extraction, RT-qPCR, and western blot

RNA and protein in cells or cerebral organoids are simultaneously extracted using the Trizol agent according to the manufacturer's protocol. The samples are incubated with 1 mL of TRIzol Reagent (Invitrogen) for lysis. Then 0.2 mL chloroform is added into the lysates. After centrifugation of 15 min, the upper aqueous phase is carefully aspirated for RNA extraction and the remaining liquid is performed for protein extraction. For RNA extraction, 0.7 volumes of isopropyl alcohol are added into the upper phase and incubated for 15 min at room temperature (RT). Then the precipitated RNA pellets are obtained and washed with 75% alcohol twice in the following 30 min centrifugation. Finally, the pellets are dissolved by RNase-free water. For protein extraction, 1.5 volumes of isopropyl alcohol is added into the leftover. After incubation for 15 min at RT, the mixtures are centrifuged for 30mins. Then the protein pellets are obtained and washed with 0.3 M HCl-guanidine three times and 100% alcohol once, respectively. Finally, the pellets are melted in 5% SDS at 55°C for 1 h. The RNA and protein are needed to be immediately put into the –80°C refrigerator for long-time preservation if not used.

For RT-qPCR, the RNA (1 µg) is reverse transcribed to cDNA using the HiScriptIII RT SuperMix of qPCR Kit (Vazyme). Then the reactions for real-time quantitative PCR (RT-qPCR) are prepared using 2×SYBR mix (Vazyme) and run on a Bio-Rad CFX Manager machine. For every gene in each sample, three replicative wells are set for detection. The primer sequences are listed in [Table S6](#).

For western blot, the protein samples are firstly run in SDS-PAGE gels (Solarbio) for separation, and then transferred to a polyvinylidene difluoride (PVDF) membrane using a cold wet transfer apparatus (BIO-RAD). Subsequently, the PVDF membrane is blocked with 5% skimmed milk solution, followed by overnight incubation with primary antibodies diluted in 5% skimmed milk solution at 4°C. On the next day, the membrane is washed three times with 1X TBST (Yamei) and incubated with horseradish peroxidase-conjugated secondary antibodies (1:5000; anti-Rabbit IgG, Jackson Immune Research; anti-Mouse IgG, Jackson Immune Research). Finally, protein bands are visualized using the Image Lab imaging system.

The primary antibodies used in this study include rabbit anti-PRMT7 (1:1000, Abcam), rabbit anti-MMA (1:1000, Cell Signaling Technology), rabbit anti-H4R3me2s (1:500, Active motif), rabbit anti-H4 (1:500, Abcam) rabbit anti-GAPDH (1:5000, AntGene), and mouse anti-tubulin (1:10000, sigma-Aldrich).

NPCs proliferation assay

Cell proliferation is assessed using cell counting kit-8 (CCK-8 kit, Beyotime) and BeyoClic EdU-555 cell proliferation kit (Beyotime). For the CCK-8 assay, 2×10^3 NPCs with *PRMT7* downregulation or not are firstly seeded into 96-well plates, with 3 replicative wells for each cell type. Post 24 h of seeding, the fresh medium with 10% CCK-8 reagent is added into each well and incubated with cells at 37°C for 4 h. Then the optical density is successively measured at 450 nm and 630 nm in a microplate reader.

For the EdU staining assay, 1.5×10^4 NPCs are seeded on the 24-well plate with pre-placed coverslips (JingAn Biological). The next day, cells are treated with EdU working solution with final concentration 10 µM for 5 h at 37°C. Subsequently, cells are fixed using 4% formaldehyde (PFA), and then permeabilized by 0.3% Triton X-100. Next, click reaction and then DNA staining are performed individually using click additive solution and Hoechst 33342. Finally, the images are captured using a confocal microscope.

Immunocytochemistry

The cells and cerebral organoid sections are performed immunofluorescence staining in our study, respectively. For cells, they are cultured in 24-well plates with pre-placed coverslips. Following three washes with PBS, the cells are fixed with 4% paraformaldehyde (PFA) for 20 min, then permeabilized with 1% Triton X-100 for 15 min, finally blocked with 5% bovine serum albumin (BSA) for 1 h. All these procedural steps are conducted at RT. For cerebral organoids, cryogenic freezing sections (16 μ m) are prepared with the assistance of liquid nitrogen, specimen molds (SAKURA), and embedding agent (SAKURA). The sections are circled using an ImmEdge Pen (VECTOR), and then performed permeabilization and blocking procedures as described above. All the above steps are performed at RT. Then, the following procedures are the same for cells and organoid sections. They are incubated with primary antibodies in 1% BSA and 0.3% Triton X-100 at 4°C for overnight. On the next day, the slices are incubated with secondary antibodies (host-specific Alexa Fluor 488/546/647) and DAPI (Beyotime) for 1 h at RT after they are washed with PBS for three times. Images are captured using a Leica SP5-2 confocal microscope equipped with a 40 \times or 20 \times objective.

The used primary antibodies in this study include rabbit anti-NESTIN (1:200, Abcam), rabbit anti-SOX2 (1:200, Cell Signaling Technologies), mouse anti-TRA-1-60 (1:200, Cell Signaling Technologies), mouse anti-SSEA4 (1:200, Cell Signaling Technologies), rabbit anti-OCT4 (1:200, Cell Signaling Technologies), rabbit anti-PAX6 (1:200, Cell Signaling Technologies), mouse anti-PAX6 (1:200, Abcam), rabbit anti-GFAP (1:200, GeneTEX), mouse anti-ki67 (1:200, Cell Signaling Technologies), rabbit anti-TUJ1 (1:200, Cell Signaling Technologies), mouse anti-TUJ1 (1:200, Cell Signaling Technologies), and rabbit anti-TBR1 (1:200, Cell Signaling Technologies).

RNA-seq and data analysis

The RNA integrity number (RIN) value and concentration are measured using Agilent 2100 Bioanalyzer. Then ribosomal RNA of the total RNA (~200 ng) is removed via Ribo-Zero Gold Kit, and the remaining RNA is used to be constructed a sequencing library according to the instruction of Illumina TruSeq Stranded Total RNA kit (Illumina). Briefly, the RNA is randomly fragmented and then reversely transcribed into cDNA. The following procedures including the second strand synthesis, dA tailing, end repairing, and PCR amplification are successively performed. Finally, the constructed RNA libraries are loaded to Illumina NextSeq500 sequencer for paired-end sequencing.

For data analysis, FastQC v0.11.2 is first used to evaluate the quality of the sequencing data. The low-quality reads are filtered via cutadapt v3.3, and then the leftover is aligned to the human reference genome Gencode GRCh38.p12 Release 29 using STAR-2.7.9a. The aligned reads are quantified through salmon-1.4.0 to obtain the original counts expression matrix. Next, voom in the limma package is used to normalize the original expression matrix. Differential gene expression analysis is subsequently performed via the linear regression model in the limma package. The differential expressed genes (DEGs) are screened as the following criteria: p value < 0.05 and $|\log_2 \text{fold change (FC)}| \geq 0.6$. The functional enrichment analysis of DEGs is performed via Database for Annotation, Visualization and Integrated Discovery (DAVID Knowledgebase v2023q3) and Metascape. The data processing software runs in R 4.2.3 environment.

Protein-protein interaction network analysis

The protein-protein interaction (PPI) network for the DEGs resulting from PRMT7 knockdown is constructed using the STRING database (v12.0). The high-confidence interactions with an interaction score > 0.7 are obtained by integrating various active interaction sources including text-mining, experiments, databases, co-expression, neighborhood, gene fusion, and co-occurrence. The final PPI network is visualized using Cytoscape (v 3.10.1).

Chromatin immunoprecipitation

The chromatin immunoprecipitation (ChIP) is performed in SH-SY5Y cell line. According to the manufacturer's protocol of SimpleChIP Enzymatic Chromatin IP Kit (Cell Signaling Technologies), the cells are first treated by 37% formaldehyde for cross-linking. Then nuclei preparation and chromatin digestion are performed to harvest fragmented genomic DNA. After analysis of chromatin digestion and concentration, the ChIP grade antibody H4R3me2s (Active motif) and IgG are individually added into the chromatin solution for overnight incubation at 4°C to pull down the DNA fragments. Following this procedure, the protein G magnetic beads are added into the solution for another 2 h incubation at 4°C. The enriched DNA fragments are then harvested through elution from the antibody-beads complex, reversal of cross-links, and final purification using spin columns. Finally, qPCR is performed in ChIP and input sample to examine whether the interesting sequence is enriched in H4R3me2s ChIP sample. The primers used in this experiment are listed in Table S6.

QUANTIFICATION AND STATISTICAL ANALYSIS

For *cis*-eQTL analysis, FastQTL is used to evaluate the association of the SNP genotype with the gene expression in GTEx portal (<https://www.gtexportal.org/home/>),⁴⁴ and Matrix eQTL is used to perform this analysis in LIBD BrianSeq phase I (<https://eqtl.org/>).

brainseq.org/phase1/eqtl/.⁴⁵ The histograms and line charts in this study are plotted via GraphPad Prism software version 10.0.2. The two-sided Student's t test is used to calculate the difference between two groups and is also performed in GraphPad Prism software. The Fisher exact test-based approach is used to assess the enrichment of PRMT7-associated DEGs in gene sets of four mental disorders. The hypergeometric distribution test is used to assess the enrichment of PRMT7-associated DEGs with SCZ organoids DEGs. p value less than 0.05 is considered statistically significant. All the statistical details of experiments can be found in the figure legends and STAR Methods, including the statistical tests used, exact value of n , what n represents, and how data are expressed.